The Phosphorus Bond

Subjects: Crystallography | Chemistry, Organic | Materials Science, Biomaterials
Contributor: Pradeep R. Varadwaj

The phosphorus bond in chemical systems, which is an inter- or intramolecular noncovalent interaction, occurs when there is evidence of a net attractive interaction between an electrophilic region associated with a covalently or coordinately bonded phosphorus atom in a molecular entity and a nucleophile in another, or the same, molecular entity. It is the second member of the family of pnictogen bonds, formed by the second member of the pnictogen family of the periodic table.

Keywords: pnictogen bonding ; phosphorus as a pnictogen bond donor ; σ- and π-hole interactions ; bonding modes ; sum of the van der Waals radii concept ; geometry analysis ; MESP analysis ; IGM-δg analysis

1. Introduction

Noncovalent interactions are one of the chemical interactions (or chemical synthons) that have been explored for some time [1][2] and continue to be elucidated [3][4]. They are yet to be fully understood because their behavior is variable from system to system [5]. The variety of these interactions is a consequence of the variability of the nature of the electron density donor and acceptor participating in the molecular assembly and therefore depends on factors such as the local geometry (bond distance and intermolecular approach angle) and the electron density profile of the interacting atomic basins. Since acid–base interactions are central to chemical reactions [6], recognition processes [7][8], bond functionalization [9], catalysis [10][11][12], and self-assembly [13][14][15], a fundamental understanding and exploration of these interactions has been one of the key issues in the rapid development of research areas such as computational chemistry [16][17][18][19], crystallography [5][20], and crystal engineering [21][22].

Noncovalent interactions show up in different flavors, including, for example, hydrogen bonding [23], halogen bonding [24], tetrel bonding [25][26][27], chalcogen bonding [28], pnictogen bonding [29][30][31][32], aerogen bonding [33], van der Waals interactions [34], and several others [35]. They are the result of attractive engagements between sites of unequal charge density and are often identified to be of Coulombic origin (a positive site attracting a negative one). Anti-electrostatic noncovalent interactions have been characterized recently [36][37]. Depending on the nature of the interacting units responsible for a molecular complex system, the extent of energy contributions due to repulsion (Pauli and electrostatic, resulting from like charges) acts against orbital interactions, polarization, and dispersion as attractive forces [36]. However, the overall stability of a system is a delicate balance between all of them, in which the overall attractive contribution to the binding energy dominates.

This overview is focused on exploring the nature of the geometric modes of pnictogen bonding, manifest in some crystals and known since the latter half of the last century but explored in greater detail more recently [38][39][40][41][42][43], addressing only phosphorus-centered pnictogen bonding (or simply, phosphorus bonding). Phosphorus, P, the second element of the pnictogen family, Group 15 of the periodic table, has an electronegativity of 2.19 on the Pauling scale, which is appreciably smaller than that of N (3.04). The most commonly observed (formal) oxidation state of phosphorus in molecules and crystals is +3 and +5, although a variety of oxidation states, from −3 to 4, are known [44]. It forms compounds with coordination numbers from 1 (as in P_2) to 9 (as in Ti_3P) [44]. Consequently, a large number of chemical systems with various oxidation states and stereochemistry are known, and the rich chemistry of P has found a wide range of uses and applications for its compounds. Here researchers demonstrate and summarize the evidence that phosphorus in molecular entities, utilizing its electrophilic character, has the ability to make attractive engagements with negative sites to form crystalline materials.

The phosphorus bond in chemical systems, which is an inter- or intramolecular noncovalent interaction, can be identified when there is evidence of a net attractive interaction between an electrophilic region associated with a covalently or coordinately bonded phosphorus atom in a molecular entity and a nucleophile in another, or the same, molecular entity. It is the second member of the family of pnictogen bonds, formed by the second member of the pnictogen family of the periodic table.

2. Illustrative Crystalline Systems

2.1. Polymorphs of Phosphorus

The group 15 elements have already started to play a role in the development of 2D semiconductor materials, including phosphorene, arsenene, antimonene, and nitrogene [45]. The terminology used for these monolayered materials is by analogy with graphene. Probably the most popular phosphorus-containing semiconducting systems (single-layered and bulk phosphorus allotropes) are single-layered Hittorf's phosphorus, Hittorfene; black phosphorus, black phosphorene; and A7 phosphorene [46]. The monolayer of novel γ-phosphorus nitride (γ-PN) was shown to be a candidate for a visible-light-driven, water-splitting photocatalyst, with an indirect bandgap transition energy of 2.85 eV, based on DFT calculations [47]. Similarly, 2D black phosphorus (a puckered material) is among the family of 2D and layered materials that have distinctive crystalline symmetries and exhibit various properties, such as high carrier mobility, strong infrared responsivity, widely tunable bandgap, in-plane anisotropy, and spontaneous electric polarization [48].

The chemical bonding holding the monolayers together in these 2D materials is often assumed to be a consequence of van der Waals forces, which are dispersive by nature. One such instance of the layered (*A7*) rhombohedral structure of phosphorus (space group *R-3m*), in which each P site in a given monolayer is bonded to three P sites in a neighboring nearest monolayer, is illustrated in **Figure 1**a.

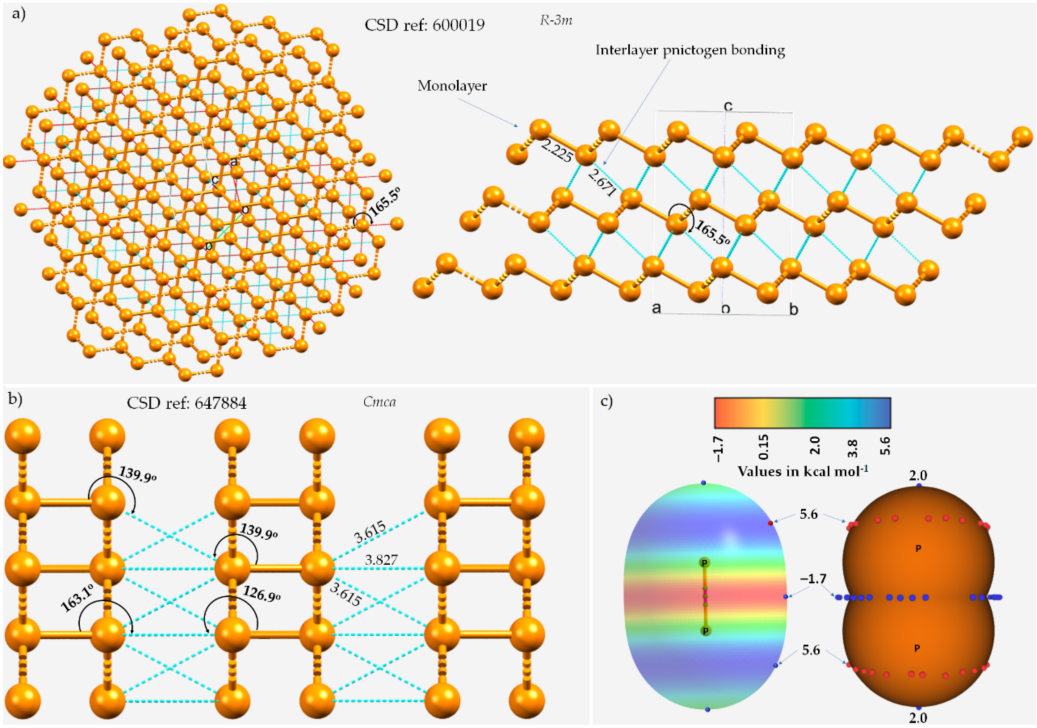

Figure 1. The ball-and-stick mode of the structure of (**a**) *A7* rhombohedral 0.19$(P_{31})_n$ crystal of phosphorus and (**b**) orthorhombic black phosphorus, showing interlayer P···P type pnictogen bonded interactions. ICSD references and space groups for each are shown. Selected bond lengths and bond angles are in Å and degrees, respectively. (**c**) The MP2(full)/aug-cc-pVTZ level 0.001 a.u. isodensity envelope mapped electrostatic potential surface of an isolated P_2 molecule. The tiny red and blue circles in (**c**) represent the local maxima and local minima of electrostatic potential ($V_{S,max}$ and $V_{S,min}$, respectively). Dotted lines in cyan represent an interaction between a pair of P atoms, and those in red, as in (**a**), represent hanging contacts. The quantum theory of atoms in molecules (QTAIM)-based molecular graphs are superimposed in (**c**), and the bond paths are in atom color, accompanied by bond critical points (tiny sphere in green). The phosphorus atoms in (**a**,**b**) are colored orange.

The three P···P intermolecular distances responsible for the interfacial region in the crystal are all equivalent, with *r*(P···P) = 2.671 Å and P–P···P = 165.5°, and appear slightly off the extension of the P–P covalent bonds (*r*(P–P) = 2.225 Å). In the case of black phosphorus, the P···P intermolecular distances between P sites of neighboring monolayers are 3.827 and 3.615 Å and are associated with ∠P–P···P contact angles of 163.1 and 139.9°, respectively (**Figure 1**b), indicative of the occurrence of Type-III and Type-I topologies of phosphorus-centered pnictogen bonding, respectively, in the crystal.

The quasilinear directional bonding features in both the crystals above may be explained using the MESP model of an isolated P_2 molecule shown in **Figure 1**c. As can be seen, the surface of the P atom in P_2 has district regions of different potential; the first is around and the second is along the P≡P bond extensions. The first region is beltlike and features

several local maxima of potential ($V_{S,max}$ ≈ 5.6 kcal mol^{-1}) that are more positive than the localized region along the P≡P bond extension ($V_{S,max}$ = 2.0 kcal mol^{-1}). The central bonding region is equipped with a belt of negative potential, with $V_{S,min}$ ≈ –1.7 kcal mol^{-1}. Clearly, there is no σ-hole observed on P along the P≡P bond extension (and this is also expected in the case of N_2). There are two local minima (but not local maxima) on the outer surfaces of the two P atoms along the P≡P bond extension that are probably the result of a buildup of relatively large charge density compared to the lateral sides of the same atoms. As such, the quasilinear nature of the P···P interlayer contacts shown in **Figure 1**a emerges because of the attraction between a pair of P sites that feature, although both positive, dissimilar charge density. In other words, these are the result of attraction between the regions on interacting P atoms described by the local minimum and maximum of potentials, which could be regarded as lump–hole interactions [49].

The crystal structure of violet phosphorus (Hittorfene) has been reported recently [50]. This layered, 2D semiconducting phosphorus allotrope (monoclinic space group) has an optical band gap of 1.7 eV. It undergoes thermal deposition at 52 °C, which is higher than the decomposition temperature of black phosphorus. The nature of P···P bonding in Hittorfene is very different from that observed in black phosphorus. One of the crucial features of Hittorfene is that each layer is bonded to the nearest layer by a number of P···P contacts with a variety of bond distances between them (**Figure 2**a). The contacts are strongly directional (∠P–P···P between 176 and 179°). There are also intralayer P···P contacts; they are markedly shorter than the interlayer contacts and are directional. They are all less than twice the vdW radius of P, 3.80 Å, and hence can be regarded as phosphorus bonds.

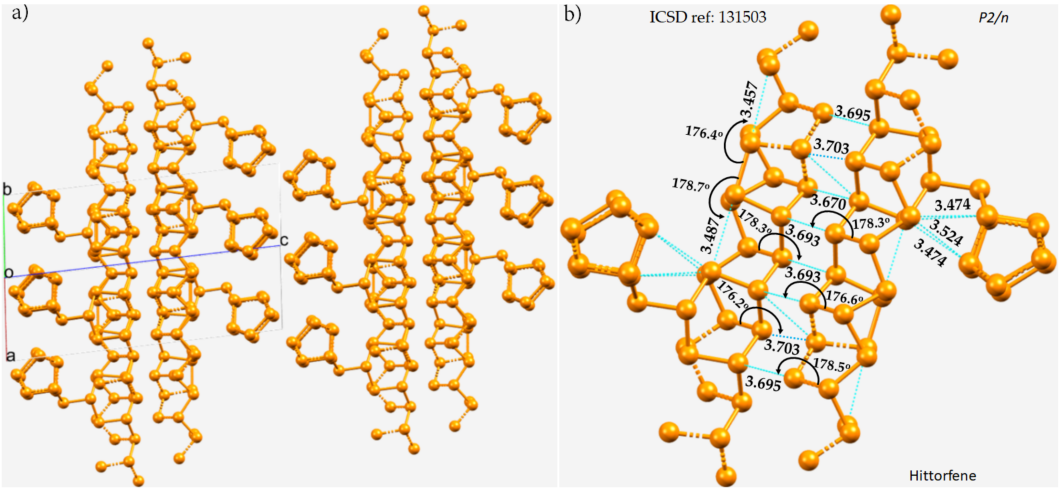

Figure 2. (**a**) The 2 × 2 × 2 supercell structure of Hittorfene (violet phosphorus). (**b**) The nature of P···P bonding interactions between the layers, and within the same layer, of the crystal. Selected bond distances and bond angles are in Å and degrees, respectively. Dotted lines in cyan represent an interaction between a pair of P atoms. P atoms in the ball-and-stick models are colored orange.

There are also a large number of phosphorus-containing crystal structures deposited in the CSD and ICSD databases. Many have been known for some considerable time, including, for example, $(P_2)_n$, ICSD ref. 647884 [51]; PCl_4, ICSD ref. 26594 [52]; PCl_5, ICSD ref. 26661 [53] and ICSD ref. 29124 [54]; PBr_5, ICSD ref. 15559 [55]; P_4S_3, ICSD ref. 16711 [56]; P_4S_5, ICSD ref. 16681 [57]; P_4S_7, ICSD ref. 23842, and P_4S_{10}, ICSD ref. 174008 [58]; $I_2P_4S_3$, ICSD ref. 26485 [59]; and $P(CN)_3$, ICSD ref. 16587 [60]. In these systems, the covalently bonded phosphorus in a given molecular entity interacts attractively with the Lewis base in partner molecule(s), thus forming phosphorus-centered pnictogen bonding and contributing to the structure of the crystals.

What follows is a description of a number of crystal systems wherein chemical bonding involving phosphorus bonds plays a structure-determining role. For many of them, researchers examined their MESP to provide insight into their Lewis acid behavior necessary for the formation of an acid–base interaction. Isolated chemical systems could serve as examples of phosphorus bonding. Chandra and coworkers [61], and others [62], have reported such chemical systems expounded from studies of isolated entities. They showed that phosphorus can serve as an acceptor of electron density from the π electron cloud in partner molecules. In particular, they have shown that the P···π phosphorus bonding interactions are responsible for the stability of the PCl_3–C_2H_2 and PCl_3–C_2H_4 heterodimers and similar trimers and tetramers generated during low-temperature measurements. The dominance of phosphorus bonding in the PCl_3–C_2H_2 and PCl_3–C_2H_4 heterodimers over other interactions (such as H···π, H···Cl, H···P, Cl···π, and lone pair–π interactions) was also discussed.

2.2. Phosphorus Trihalides

Phosphorus trihalides, PX_3 (X = F, Cl, Br, I), are probably the simplest tetra-atomic molecular systems that can be used to arrive at an understanding of phosphorus-centered pnictogen bonding in crystals. The ωB97XD/Jorge-ATZP computed MESP plots for PX_3 (X = F, Cl, Br, I) are compared in **Figure 3**. Except for F in PF_3 (**Figure 3**a), the halogen derivative X has a charge density depletion region on the outer extensions of the P–X covalent bond that increases as the electronegativity decreases in the series from Cl through Br to I. Associated with these depleted charge density regions are σ-holes on the halogen derivatives, whose strength increases in the opposite order: P–Cl (10.0 kcal mol^{-1}) < P–Br (16.1 kcal mol^{-1}) < P–I (17.0 kcal mol^{-1}), concordant with an increase in the polarizability of X. The apparent absence of a σ-hole on F in PF_3 is not unexpected and has been observed in other chloro- and fluorinated compounds [63][64][65][66].

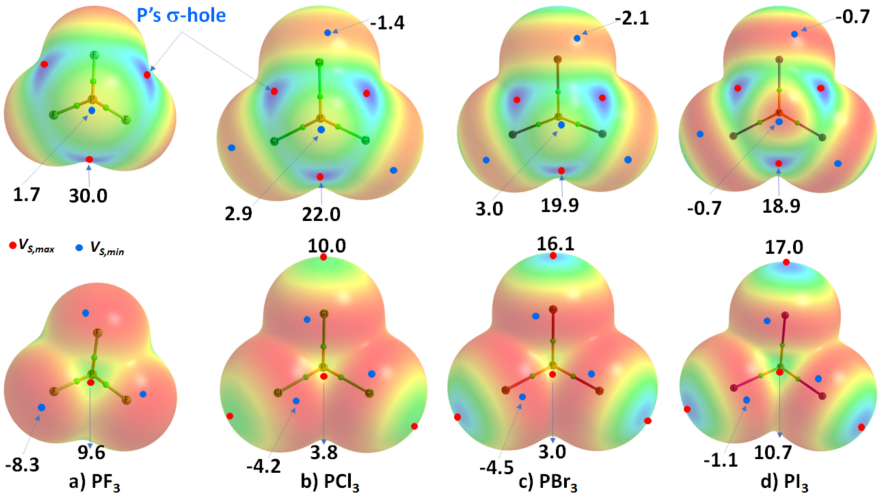

Figure 3. Comparison of ωB97XD/Jorge-ATZP calculated 0.001 a.u. isodensity envelope mapped potential on the electrostatic surfaces of PX_3 (X = (**a**) F, (**b**) Cl, (**c**) Br, (**d**) I) molecules. Selected tiny circles in red and blue describing $V_{S,max}$ and $V_{S,min}$ values in kcal mol^{-1} are shown, which are the local maxima and minima of potential, respectively. Two views of each MESP graph are displayed for each molecule. Top: coordinated P faces the reader. Bottom: the three X atoms forming a triangular architecture face the reader. The QTAIM-based molecular graphs are superimposed on each case, and the bond paths are in atom color, accompanied by bond critical points (tiny sphere in green).

On the other hand, the strength of the σ-hole on P decreases as X proceeds from F down to I and so is most stable along the outermost X–P bond extensions when X = F. This is expected given that F is the most electronegative and least polarizable of the halogens. It therefore has a very high ability to pull electron density on P towards the bonding region in the P–F bonds, thus leaving a strongly positive potential on the surface of covalently bonded P.

Researchers observe that the σ-hole regions on covalently bonded X are more positive than the lateral portions in PX_3. The latter is described by a belt of negative potential. Except for PF_3, the belt is not equipotential as can be inferred from the color of the belt. For example, the potential around the lateral site shown in the top view of **Figure 3**b–d is colored orange ($V_{S,min}$ roughly −1.4 kcal mol^{-1} for PCl_3), and that shown in the bottom view is colored red ($V_{S,min}$ ~ −8.3 kcal mol^{-1} for PCl_3). The P site in PX_3 (X = F, Cl, Br, with I being the exception) is entirely positive (i.e., both $V_{S,max}$ > 0 and $V_{S,min}$ > 0). These results suggest that the lateral and axial sides, respectively, of halogen derivatives in a given PX_3 molecule might be capable of making an attractive engagement with the axial and lateral sites, respectively, of another molecule of the same type to form $X_3P\cdots PX_3$ complexes, as researchers point out below.

While the (arbitrary) use of the 0.001 a.u. isodensity envelope is often recommended for computing electrostatic potential [67][68], it may not always be appropriate [63][64][65]. Its use in the present case, for instance, suggested that $V_{S,max}$ is neutral on the extensions of the three P–F bonds in PF_3. Moreover, it is expected that the region dominated by the lone pairs on F, located around the lateral sites of the P–F bond, should be accompanied by at least three critical points of potential, $V_{S,min}$. However, researchers' calculation gave a single local minimum of potential on each F, with $V_{S,min}$ of –8.3 kcal mol^{-1}, and a positive minimum of $V_{S,min}$ of +1.8 kcal mol^{-1} on P. Researchers' calculation also gave three, nearly equivalent $V_{S,max}$ on P of 30.0 kcal mol^{-1} on P along F–P bond extensions, and one on the central region formed by the triangular face formed by three F atoms, with $V_{S,max}$ of +9.3 kcal mol^{-1}. Although most of the positive and negative regions on the surface of the PF_3 originated from a mapping of the 0.001 a.u. isoelectron density envelope, it failed to provide any insight as to whether a covalently bonded F atom in the molecule has a σ-hole on the P–F bond extensions.

Researchers explored the MESP of PF_3 generated with different isodensity envelopes. These led to the emergence of the expected potential profile on the axial portion of P–F bond extensions. Specifically, two (three) local maxima of potential appeared only when researchers used a 0.0037 a.u. (0.0038 a.u.) isoelectron density envelope ($V_{S,max}$ = −5.5 kcal mol^{-1}), showing that F in PF_3 does indeed have a negative σ-hole. The values of $V_{S,max}$ and $V_{S,min}$ calculated using three different isoelectron density envelopes are shown in **Figure 4**. The actual nature of the potential on the molecular electrostatic surface of the PF_3 was obtained only when the 0.0038 a.u. isodensity envelope was used. Because $V_{S,max}$ and $V_{S,min}$ on F along and around the P–F bond extensions are both negative regardless of the isodensity envelops used, it is clear that F can act as a versatile pnictogen bond acceptor.

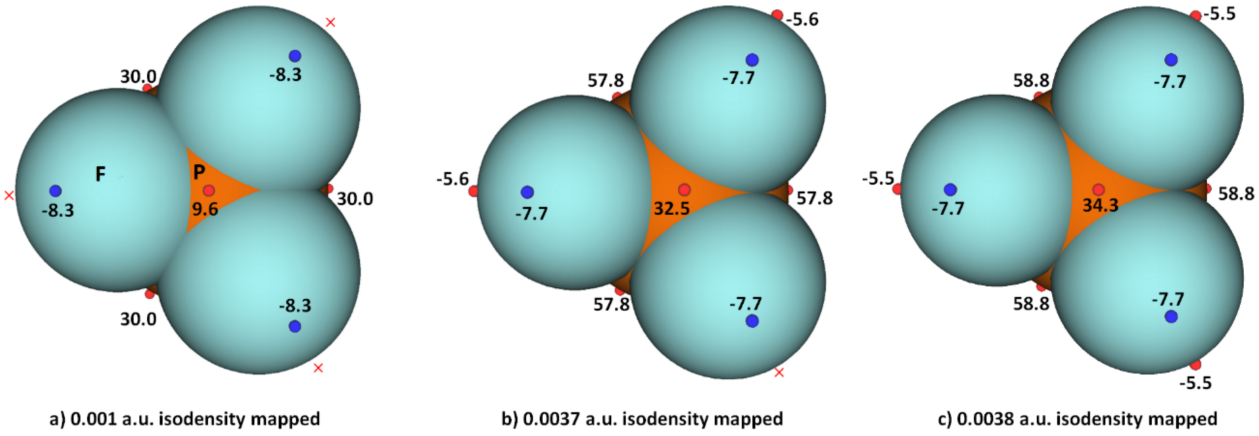

Figure 4. Comparison of ωB97XD/Jorge-ATZP level computed local maxima and minima of electrostatic potential of PF_3 mapped on three different isoelectron density surfaces ((**a**) 0.001 a.u.; (**b**) 0.0037 a.u.; (**c**) 0.0038 a.u.), showing the dependence of $V_{S,max}$ and $V_{S,min}$ on the value of isodensity envelope used. The red crosses indicate the missing maxima on covalently bonded F. The tiny circles in red and blue represent the $V_{S,max}$ and $V_{S,min}$, respectively. Values in kcal mol^{-1}.

Because of the inconsistencies above, researchers recalculated the electrostatic potential using the def2-TZVPD basis set, in conjunction with MP2(full). All the monomers were optimized at this level of theory, and the wavefunctions were then evaluated at the same level. The results are summarized in **Figure 5** and **Table 1**. The data show that the 0.001 a.u. isodensity envelope is not a suitable choice on which to compute the potential since it is not ideal to elucidate the van der Waals surface of the PF_3 molecule. When at least a 0.0028 a.u. isodensity envelope was used for computing the potential, all the expected critical points of the potential showed up on the surfaces of the three F atoms of the PF_3 molecule along the P–F bond extensions, as observed on surfaces of X of the other three PX_3 molecules (**Figure 5**). All three σ-holes on the three F atoms in PF_3 are found to be entirely negative ($V_{S,max}$ = –5.3 kcal mol^{-1}), surrounded by a belt of negative sites around their lateral portions.

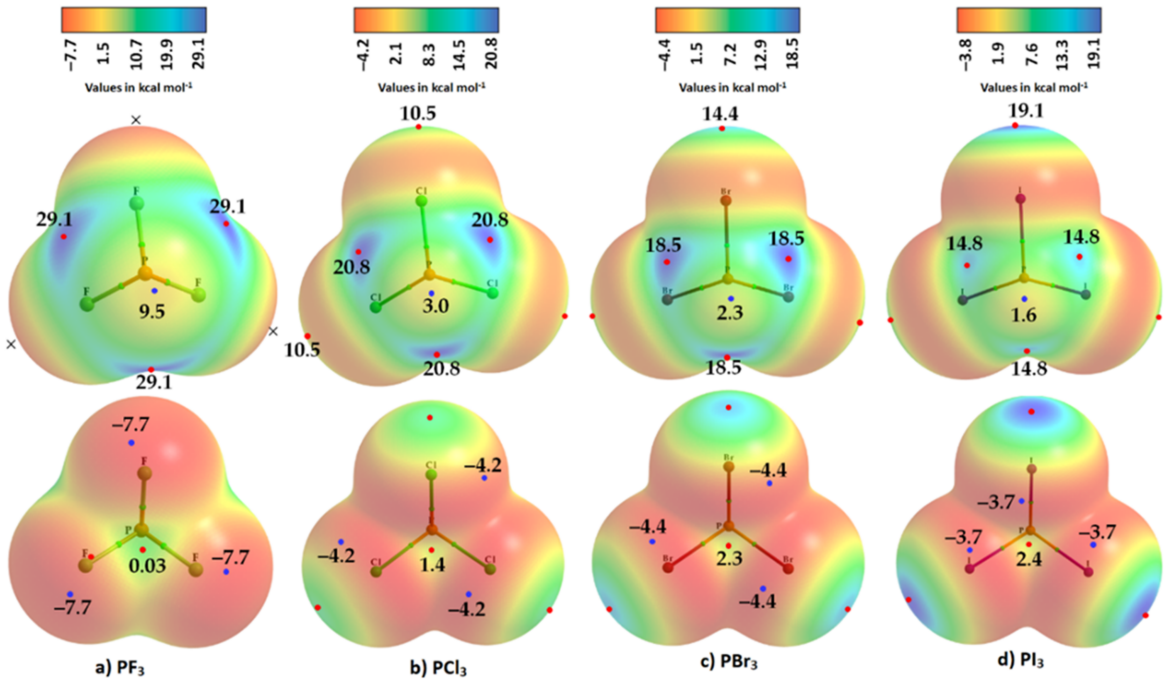

Figure 5. Comparison of MP2(full)/def2-TZVPD calculated 0.001 a.u. isodensity envelope mapped potential on the electrostatic surfaces of PX_3 (X = (**a**) F, (**b**) Cl, (**c**) Br, (**d**) I) molecules. Selected $V_{S,max}$ and $V_{S,min}$ values in kcal mol^{-1} are shown, which are the local maxima and minima of potential, respectively. Two views of each MESP graph for each molecule are displayed: (Top) Covalently bonded P faces the reader. (Bottom) The three X atoms forming a triangular architecture face the reader. The QTAIM-based molecular graphs are superimposed on each case, and the bond paths are in atom color, accompanied by bond critical points (tiny sphere in green).

Table 1. The 0.001 a.u. isodensity envelope mapped potential on the electrostatic surface of PX_3 (X = F, Cl, Br, I) molecules, obtained using MP2(full)/def2-TZVPD [a].

Local Extrema on the Surface of Specific Atom/Bond	PF_3	PF_3	PCl_3	PBr_3	PI_3
	0.001 a.u.	0.0028 a.u.	0.001 a.u.	0.001 a.u.	0.001 a.u.
$V_{s,min}$ On X (lateral portions)	−7.7	−7.5	−4.2	−4.4	−3.7
$V_{s,min}$ On X (lateral portions)	−7.7	−7.5	−4.2	−4.4	−3.7
$V_{s,min}$ On X (lateral portions)	−7.7	−7.5	−4.2	−4.4	−3.7
$V_{s,min}$ on P (opposite to the triangular face formed by three X atoms)	0.03	0.1	1.4	2.3	1.6
$V_{S,max}$ (on P−X bond extensions)	-	−5.3	10.5	14.4	19.1
$V_{S,max}$ (on P−X bond extensions)	-	−5.3	10.5	14.3	19.1
$V_{S,max}$ (on P−X bond extensions)	29.1	−5.3	10.5	14.4	19.1
$V_{S,max}$ (on X−P bond extensions)	29.1	48.9	20.7	18.5	14.9
$V_{S,max}$ (on X−P bond extensions)	29.1	48.9	20.8	18.5	14.8
$V_{S,max}$ (on X−P bond extensions)	9.5	48.9	20.8	18.4	14.8
$V_{S,max}$ (on the centroid of the triangular face formed by three X atoms)	-	26.0	3.0	2.3	2.4

[a] The 0.0028 a.u. isodensity envelope mapped potential on the electrostatic surface of PF_3 molecule is included to show that the σ-hole on F in this molecule is not neutral.

The σ-holes on X in PX_3 (X = Cl, Br, I) are found to be positive, increasing in magnitude with the polarizability of X: Cl (10.5 kcal mol^{-1}) < Br (14.4 kcal mol^{-1}) < I (19.1 kcal mol^{-1}). This is opposite to the trend found for the π-hole on the P atom in these molecules, as well as of the σ-hole on the P atom along the X–P bond extensions—a trend which is very similar to that of the $V_{S,min}$ around the halogen atoms in the series (PF_3 > PCl_3 > PBr_3 > PI_3). Totals of 10 and 14 local minima, respectively, were found on the surfaces of PCl_3 and PBr_3; these minima were significantly larger than those on PF_3 and PI_3 (not shown). These results show that the choice of an appropriate basis set and an isodensity envelope is important in determining the correct nature of local surface extrema and hence in being able to deduce the reactivity of a specific atomic domain in a molecular entity.

A crystalline structure of PF_3 is unavailable; its molecular structure has been reported by gas-phase electron diffraction [69]. Crystalline PCl_3 has been reported (at −110 °C, ICSD ref. 32027 [70], and at −150 °C, ICSD ref. 27798 [71]; Z = 4; space group *Pnma*), as has PBr_3 (ICSD ref. 8052, Z = 2, space group *Pnma* [72]) and PI_3 (ICSD ref. 311, Z = 4, space group $P6_3$ [73]).

In a simple Lewis structure of each of these molecules, trivalent P is σ-bonded with three halogens in a triangular pyramidal structure, with a lone pair on the phosphorus atom and with three lone pairs on each halogen. The crystal structures of PX_3 (X = Cl, Br, I) are shown in **Figure 6**. In each case, the P···X and X···X intermolecular bonding modes are illustrated. The average P···X bond distance is longer than the average X···X bond distance in PCl_3 and PBr_3. Each P site in these two structures is involved in five P···X contacts with the surrounding molecules, showing a similar pattern of intermolecular pnictogen bonding environment in both the crystals. Two of these contacts are quasilinear and the other three are nonlinear. For instance, a pair of two quasilinear Type-II interactions in PCl_3 have ∠P–Cl···Cl = 175.3°, and the nonlinear Type-II interactions have ∠P–Cl···Cl = 143.2°. The corresponding values in PBr_3 are 171.4 and 122.9°, respectively.

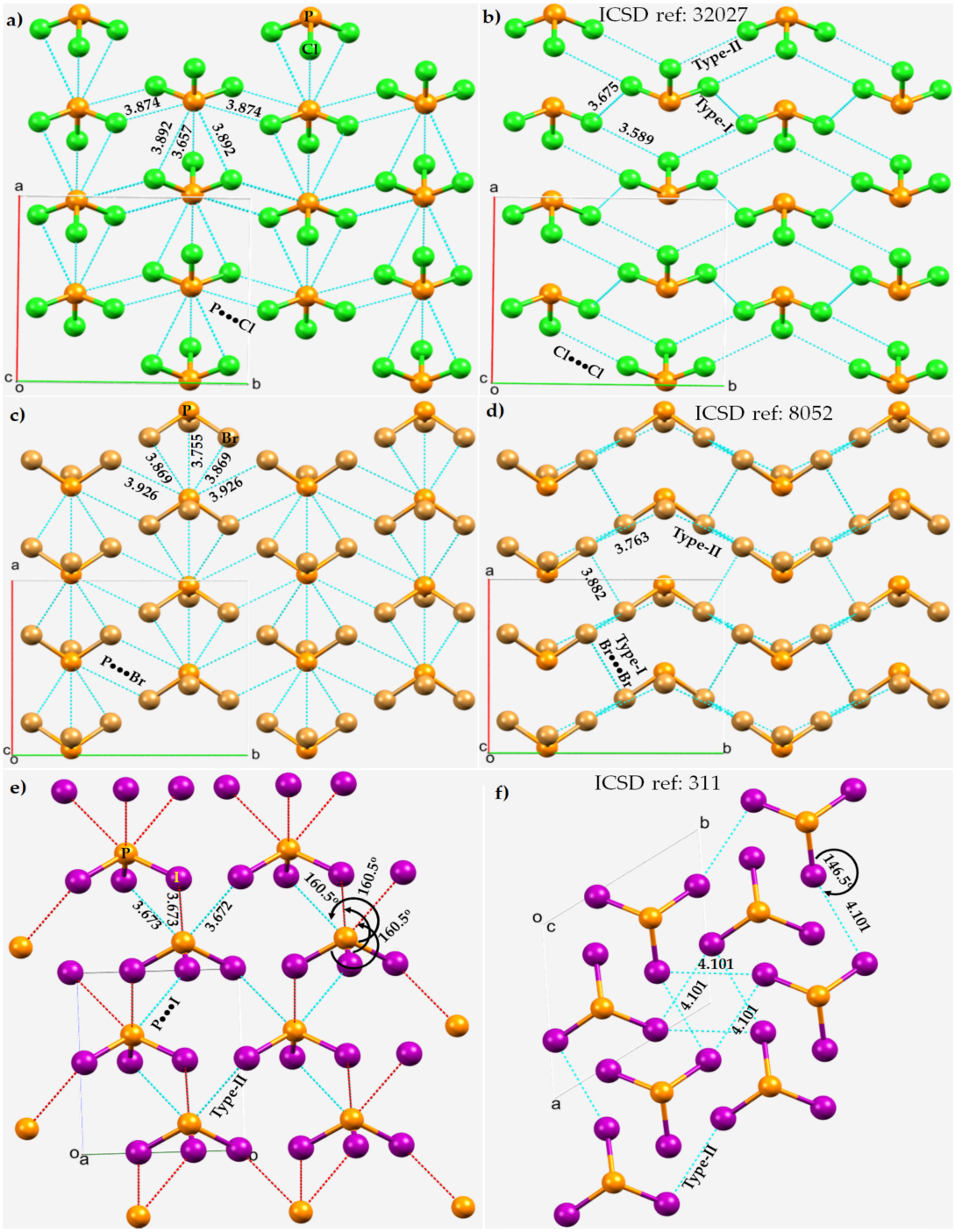

Figure 6. P···X and X···X bonding modes in the 2 × 2 × 2 supercell crystal structure of PX_3 (X = Cl, Br, I). Selected bond lengths and bond angles are in Å and degrees, respectively. Atom type is shown in each case. (**a**) P···Cl and (**b**) Cl···Cl in PCl_3. (**c**) P···Br and (**d**) Br···Br in in PBr_3. (**e**) P···I and (**f**) I···I in PI_3.

The short Cl···P contact in PCl_3 at 3.657 Å and P–Cl···P of 171.4° (**Figure 6**a) may not be a pnictogen bond since the positive potential on P ($V_{S,min}$ = 3.0 kcal mol^{-1}) in one molecule is weaker than that of the interacting Cl atom in the partner molecule along the P–Cl bond extension ($V_{S,max}$ = 10.5 kcal mol^{-1}). This interaction is more likely a Type-III halogen bond [74], which occurs between interacting sites that feature a very similar directional behavior to a Type-II interaction, but are formed between sites with potentials of identical sign. The short P···Br contact in PBr_3 at 3.755 Å with ∠P–Br···P = 126.8° between positive P and negative Br (**Figure 6**c) is nonlinear and is probably a π-centered pnictogen bonding interaction. Researchers note further that each PBr_3 molecular unit in the crystal is also bonded to another PBr_3 (back-to-back in **Figure 6**c, but not visible) via a Br···P contact, with a bond distance and ∠P–Br···P of 4.329 Å and 158.7°, respectively (not shown). Its characteristic is similar to those of the corresponding Cl···P interactions observed in the PCl_3 crystal, and hence researchers attribute this to a Type-II halogen bond.

Although the Type-II Br···Br noncovalent links force the PBr_3 molecules to produce a zig-zag pattern along the crystallographic *b*-direction, they are weak and possibly dispersion-driven since the intermolecular distances associated with these interactions (r(Br···Br) = 3.763 Å) are slightly larger than twice the vdW radius of Br, 3.72 Å. This does not necessarily mean that the contribution due to electrostatics is negligible; the overall stability of these weak interactions

may be understood as a delicate balance between attractive and repulsive forces. In any case, each covalently bonded Br is involved in forming at least four Br···Br contacts. Three of them are Type-I, with *r*(Br···Br) 3.766 or 3.882 Å. These are also expected to be weaker than, or of comparable strength to, the Type-II Br···Br contacts in PBr_3. A similar conclusion may be drawn in the case of the PCl_3 system when the P···Cl and Cl···Cl contacts are compared.

The nature of the noncovalent bonding deduced for PCl_3 and PBr_3 is different in crystalline PI_3, as can be inferred by comparing the Type-II P···I and I···I bond distances shown in **Figure 6**e,f, respectively. For the latter system, the P···I contacts appear to be more Coulombic in nature and the I···I contacts are dispersion-driven and weak, since *r*(P···I = 3.673 Å) is significantly shorter than the sum of the vdW radii of P and I, 3.94 Å. Similarly, the I···I intermolecular distances, *r*(I···I) = 4.101 Å, are slightly larger than twice the vdW radius of I, 4.08 Å, and are nonlinear (∠P–I···I =146.5°).

It is evident that the Type-II P···X and X···X pnictogen bonding and halogen bonding modes interplay to stabilize the crystals; they can be explained by means of the MESP models of isolated PX_3 molecules (see above). However, this model fails to explain the Type-I X···X interactions regardless of the chemical system investigated since these interactions generally occur between negative lateral sites on a covalently bonded halogen derivative that attract each other when interacting molecular entities are in close proximity.

References

1. Etter, M.C. Encoding and decoding hydrogen-bond patterns of organic compounds. Acc. Chem. Res. 1990, 23, 120–126.
2. Etter, M.C.; Urbanczyk-Lipkowska, Z.; Zia-Ebrahimi, M.; Panunto, T.W. Hydrogen bond-directed cocrystallization and molecular recognition properties of diarylureas. J. Am. Chem. Soc. 1990, 112, 8415–8426.
3. Johnson, E.R.; Keinan, S.; Mori-Sánchez, P.; Contreras-García, J.; Cohen, A.J.; Yang, W. Revealing Noncovalent Interactions. J. Am. Chem. Soc. 2010, 132, 6498–6506.
4. Desiraju, G.R. A Bond by Any Other Name. Angew. Chem. Int. Ed. 2011, 50, 52–59.
5. Desiraju, G.R.; Steiner, T. The Weak Hydrogen Bond in Structural Chemistry and Biology (International Union of Crystallography Monographs on Crystallography, 9); Oxford University Press: Oxford, UK; New York, NY, USA, 1999.
6. Ishikita, H.; Saito, K. Proton transfer reactions and hydrogen-bond networks in protein environments. J. Roy. Soc. Interface 2014, 11, 20130518.
7. Dongfang, J.; Tingting, S.; Huan, C.; Xufeng, S.; Yu Yanmin, Y. Non-covalent interactions in molecular recognition of porphyrins. Mater. Rev. 2018, 32, 3068–3075.
8. Motherwell, W.B.; Moreno, R.B.; Pavlakos, I.; Arendorf, J.R.T.; Arif, T.; Tizzard, G.J.; Coles, S.J.; Aliev, A.E. Noncovalent Interactions of π Systems with Sulfur: The Atomic Chameleon of Molecular Recognition. Angew. Chem. Int. Ed. 2018, 57, 1193–1198.
9. Mahmudov, K.T.; Gurbanov, A.V.; Guedes da Silva, M.F.C.; Pombeiro, A.J.L. Noncovalent Interactions in C–H Bond Functionalization. In Noncovalent Interactions in Catalysis; Chapter 1; Mahmudov, K.T., Kopylovich, M.N., Guedes da Silva, M.F.C., Pombeiro, A.J.L., Eds.; Royal Society of Chemistry: London, UK, 2019; pp. 1–25.
10. Berger, G.; Frangvillea, P.; Meyer, F. Halogen bonding for molecular recognition: New developments in materials and biological science. Chem. Commun. 2020, 56, 4970–4981.
11. Yan, W.; Zheng, M.; Xu, C.; Chen, F.-E. Harnessing noncovalent interaction of chalcogen bond in organocatalysis: From the catalyst point of view. Green Synth. Cat. 2021, 2, 329–336.
12. Paraja, M.; Gini, A.; Sakai, N.; Matile, S. Pnictogen-Bonding Catalysis: An Interactive Tool to Uncover Unorthodox Mechanisms in Polyether Cascade Cyclizations. Chem. Eur. J. 2020, 26, 15471–15476.
13. Liu, Y.F.; Zhang, L.; Wei, W. Effect of noncovalent interaction on the self-assembly of a designed peptide and its potential use as a carrier for controlled bFGF release. Int. J. Nanomed. 2017, 12, 659–670.
14. Subramani, K.; Ahmed, W. Self-Assembly of Proteins and Peptides and Their Applications in Bionanotechnology and Dentistry. In Emerging Nanotechnologies in Dentistry; Chapter 13; Subramani, K., Ahmed, W., Eds.; William Andrew Publishing: Boston, MA, USA, 2012; pp. 209–224.
15. Fung, S.Y.; Hong, Y.; Keyes-Baig, C.; Chen, P. 12—Self-assembly of peptides and its potential applications. In Molecular Interfacial Phenomena of Polymers and Biopolymers; Chen, P., Ed.; Woodhead Publishing, CRC Press: Boca Raton, FL, USA, 2005; pp. 421–474.

16. Zhao, Y.; Truhlar, D.G. Density Functionals for Noncovalent Interaction Energies of Biological Importance. J. Chem. Theory Comp. 2007, 3, 289–300.
17. Corminboeuf, C. Minimizing Density Functional Failures for Non-Covalent Interactions beyond van der Waals Complexes. Acc. Chem. Res. 2014, 47, 3217–3224.
18. Burns, L.A.; Vázquez-Mayagoitia, Á.; Sumpter, B.G.; Sherrill, C.D. Density-functional approaches to noncovalent interactions: A comparison of dispersion corrections (DFT-D), exchange-hole dipole moment (XDM) theory, and specialized functionals. J. Chem. Phys. 2011, 134, 84107.
19. Gao, T.; Li, H.; Li, W.; Li, L.; Fang, C.; Li, H.; Hu, L.; Lu, Y.; Su, Z.-M. A machine learning correction for DFT non-covalent interactions based on the S22, S66 and X40 benchmark databases. J. Cheminform. 2016, 8, 24.
20. Mahmudov, K.T.; Gurbanov, A.V.; Aliyeva, V.A.; Resnati, G.; Pombeiro, A.J.L. Pnictogen bonding in coordination chemistry. Coord. Chem. Rev. 2020, 418, 213381.
21. Desiraju, G.R. Hydrogen bridges in crystal engineering: Interactions without borders. Acc. Chem. Res. 2002, 35, 565–573.
22. Ganguly, P.; Desiraju, G.R. Van der Waals and Polar Intermolecular Contact Distances: Quantifying Supramolecular Synthons. Chem. Asian J. 2008, 3, 868–880.
23. Arunan, E.; Desiraju, G.R.; Klein, R.A.; Sadlej, J.; Scheiner, S.; Alkorta, I.; Clary, D.C.; Crabtree, R.H.; Dannenberg, J.J.; Hobza, P.; et al. Definition of the hydrogen bond (IUPAC Recommendations 2011). Pure Appl. Chem. 2011, 83, 1637–1641.
24. Desiraju, G.R.; Shing Ho, P.; Kloo, L.; Legon, A.C.; Marquardt, R.; Metrangolo, P.; Politzer, P.; Resnati, G.; Rissanen, K. Definition of the halogen bond (IUPAC Recommendations 2013). Pure Appl. Chem. 2013, 85, 1711–1713.
25. Bauzá, A.; Mooibroek, T.J.; Frontera, A. Tetrel-Bonding Interaction: Rediscovered Supramolecular Force? Angew. Chem. Int. Ed. 2013, 52, 12317–12321.
26. Taylor, P.G.; Bassindale, A.R.; El Aziz, Y.; Pourny, M.; Stevenson, R.; Hursthouse, M.B.; Coles, S.J. Further studies of fluoride ion entrapment in octasilsesquioxane cages; X-ray crystal structure studies and factors that affect their formation. Dalton Trans. 2012, 41, 2048–2059.
27. Varadwaj, P.R.; Varadwaj, A.; Jin, B.Y.Y. Significant evidence of C···O and C···C long-range contacts in several heterodimeric complexes of CO with CH3-X, should one refer to them as carbon and dicarbon bonds! Phys. Chem. Chem. Phys. 2014, 16, 17238–17252.
28. Aakeroy, C.B.; Bryce, D.L.; Desiraju, R.G.; Frontera, A.; Legon, A.C.; Nicotra, F.; Rissanen, K.; Scheiner, S.; Terraneo, G.; Metrangolo, P.; et al. Definition of the chalcogen bond (IUPAC Recommendations 2019). Pure Appl. Chem. 2019, 91, 1889–1892.
29. Frontera, A.; Bauza, A. On the Importance of Pnictogen and Chalcogen Bonding Interactions in Supramolecular Catalysis. Int. J. Mol. Sci. 2021, 22, 12550.
30. Trubenstein, H.J.; Moaven, S.; Vega, M.; Unruh, D.K.; Cozzolino, A.F. Pnictogen bonding with alkoxide cages: Which pnictogen is best? New J. Chem. 2019, 43, 14305–14312.
31. Lindquist-Kleissler, B.; Wenger, J.S.; Johnstone, T.C. Analysis of Oxygen–Pnictogen Bonding with Full Bond Path Topological Analysis of the Electron Density. Inorg. Chem. 2021, 60, 1846–1856.
32. De Azevedo Santos, L.; van der Lubbe, S.C.C.; Hamlin, T.A.; Ramalho, T.C.; Matthias Bickelhaupt, F. A Quantitative Molecular Orbital Perspective of the Chalcogen Bond. ChemistryOpen 2021, 10, 391–401.
33. Bauzá, A.; Frontera, A. Aerogen Bonding Interaction: A New Supramolecular Force? Angew. Chem. Int. Ed. 2015, 54, 7340–7343.
34. Steiner, T.; Desiraju, G.R. Distinction between the weak hydrogen bond and the van der Waals interaction. Chem. Commun. 1998, 891–892.
35. Frontera, A.; Bauzá, A. On the Importance of σ–Hole Interactions in Crystal Structures. Crystals 2021, 11, 1205.
36. Holthoff, J.M.; Engelage, E.; Weiss, R.; Huber, S.M. “Anti-Electrostatic” Halogen Bonding. Angew. Chem. Int. Ed. 2020, 59, 11150–11157.
37. Loy, C.; Holthoff, J.M.; Weiss, R.; Huber, S.M.; Rosokha, S.V. “Anti-electrostatic” halogen bonding in solution. Chem. Sci. 2021, 12, 8246–8251.
38. Carré, F.; Chuit, C.; Corriu, R.J.P.; Monforte, P.; Nayyar, N.K.; Reyé, C. Intramolecular coordination at phosphorus: Donor-acceptor interaction in three- and four-coordinated phosphorus compounds. J. Organomet. Chem. 1995, 499, 147–154.

39. Ashe, A.J. Thermochromic Distibines and Dibismuthines. In Advances in Organometallic Chemistry; Stone, F.G.A., West, R., Eds.; Academic Press: San Diego, CA, USA, 1990; Volume 30, pp. 77–97.

40. Del Bene, J.; Alkorta, I.; Elguero, J. The Pnicogen Bond in Review: Structures, Binding Energies, Bonding Properties, and Spin-Spin Coupling Constants of Complexes Stabilized by Pnicogen Bonds. In Noncovalent Forces. Challenges and Advances in Computational Chemistry and Physics; Scheiner, S., Ed.; Springer: Cham, Switzerland, 2015; Volume 19.

41. Joshi, P.R.; Sankaran, K. P···N type pnicogen bonding in phosphorus trichloride–pyridine adduct: A matrix isolation infrared, DFT and ab initio study. J. Mol. Str. 2020, 1217, 128408.

42. Mokrai, R.; Barrett, J.; Apperley, D.C.; Batsanov, A.S.; Benkő, Z.; Heift, D. Weak Pnictogen Bond with Bismuth: Experimental Evidence Based on Bi−P Through-Space Coupling. Chem. Eur. J. 2019, 25, 4017–4024.

43. De Azevedo Santos, L.; Hamlin, T.A.; Ramalho, T.C.; Bickelhaupt, F.M. The pnictogen bond: A quantitative molecular orbital picture. Phys. Chem. Chem. Phys. 2021, 23, 13842–13852.

44. Greenwood, N.N.; Earnshaw, A. Chemistry of the Elements, 2nd ed.; Elsevier: Oxford, UK, 1997.

45. Xiao, H.; Hao, F.; Liao, X.; Shi, X.; Zhang, Y.; Chen, X. Prediction of a Two-Dimensional Phosphorus Nitride Monolayer (v2). Available online: https://arxiv.org/abs/1603.01957v2 (accessed on 29 December 2021).

46. Schusteritsch, G.; Uhrin, M.; Pickard, C.J. Single-Layered Hittorf's Phosphorus: A Wide-Bandgap High Mobility 2D Material. Nano Lett. 2016, 16, 2975–2980.

47. Tan, X.; Ji, Y.; Dong, H.; Liu, M.; Hou, T.; Li, Y. A novel metal-free two-dimensional material for photocatalytic water splitting—Phosphorus nitride (γ-PN). RSC Adv. 2017, 7, 50239–50245.

48. Xia, F.; Wang, H.; Hwang, J.C.M.; Neto, A.H.C.; Yang, L. Black phosphorus and its isoelectronic materials. Nat. Rev. Phys. 2019, 1, 306–317.

49. Eskandari, K.; Zariny, H. Halogen bonding: A lump-hole interaction. Chem. Phys. Lett. 2010, 492, 9–13.

50. Zhang, L.; Huang, H.; Zhang, B.; Gu, M.; Zhao, D.; Zhao, X.; Li, L.; Zhou, J.; Wu, K.; Cheng, Y.; et al. Structure and Properties of Violet Phosphorus and Its Phosphorene Exfoliation. Angew Chem. Int. Edn. 2020, 59, 1074–1080.

51. Krebs, H.; Holz, W.; Worms, K.H. Über die Struktur und die Eigenschaften der Halbmetalle, X. Eine Neue Rhombische Arsenmodifikation und Ihre Mischkristallbildung mit Schwarzem Phosphor. Chem. Ber. 1957, 90, 1031–1037.

52. Zelezny, W.F.; Baenziger, N.C. The Crystal Structure of Tetrachlorophosphonium Dichloroiodide. J. Am. Chem. Soc. 1952, 74, 6151–6152.

53. Clark, D.; Powell, H.M.; Wells, A.F. 134. The crystal structure of phosphorus pentachloride. J. Chem. Soc. 1942, 642–645.

54. Powell, H.M.; Clark, D.; Wells, A.F. Crystal Structure of Phosphorus Pentachloride. Nature 1940, 145, 149.

55. Van Driel, M.; Mac Gillavry, C.H. The crystal structure of phosphorus pentabromide. Rec. Trav. Chim. Pays-Bas 1943, 62, 167–171.

56. Leung, Y.C.; Waser, J.; Houten, S.v.; Vos, A.; Wiegers, G.A.; Wiebenga, E.H. The crystal structure of P4S3. Acta Crystallogr. 1957, 10, 574–582.

57. Van Houten, S.; Wiebenga, E.H. The crystal structure of P4S5. Acta Crystallogr. 1957, 10, 156–160.

58. Vos, A.; Wiebenga, E.H. The crystal structures of P4S10 and P4S7. Acta Crystallogr. 1955, 8, 217–223.

59. Wright, D.A.; Penfold, B.R. The crystal and molecular structure of phosphorus thioiodide. Acta Crystallogr. 1959, 12, 455–460.

60. Emerson, K. The crystal and molecular structure of sulfur dicyanide. Acta Crystallogr. 1966, 21, 970–974.

61. Chandra, S.; Suryaprasad, B.; Ramanathan, N.; Sundararajan, K. Dominance of unique P···π phosphorus bonding with π donors: Evidence using matrix isolation infrared spectroscopy and computational methodology. Phys. Chem. Chem. Phys. 2020, 22, 20771–20791.

62. Legon, A.C. Tetrel, pnictogen and chalcogen bonds identified in the gas phase before they had names: A systematic look at non-covalent interactions. Phys. Chem. Chem. Phys. 2017, 19, 14884–14896.

63. Varadwaj, A.; Marques, H.M.; Varadwaj, P.R. Is the Fluorine in Molecules Dispersive? Is Molecular Electrostatic Potential a Valid Property to Explore Fluorine-Centered Non-Covalent Interactions? Molecules 2019, 24, 379.

64. Varadwaj, A.; Marques, H.M.; Varadwaj, P.R. Nature of halogen-centered intermolecular interactions in crystal growth and design: Fluorine-centered interactions in dimers in crystalline hexafluoropropylene as a prototype. J. Comp. Chem. 2019, 40, 1836–1860.

65. Varadwaj, P.R.; Varadwaj, A.; Marques, H.M. Does Chlorine in CH3Cl Behave as a Genuine Halogen Bond Donor? Crystals 2020, 10, 146.
66. Varadwaj, A.; Varadwaj, P.R.; Jin, B.-Y. Fluorines in tetrafluoromethane as halogen bond donors: Revisiting address the nature of the fluorine's σ-hole. Int. J. Quantum Chem. 2015, 115, 453–470.
67. Politzer, P.; Murray, J.S.; Yepes, D.; Jaque, P. Driving and retarding forces in a chemical reaction. J. Mol. Model. 2014, 20, 2351.
68. Esrafili, M.D.; Ghanbari, M.; Mohammadian-Sabet, F. Substituent effects on cooperativity of pnicogen bonds. J. Mol. Model. 2014, 20, 2436.
69. Morino, Y.; Kuchitsu, K.; Moritani, T. Molecular structure of phosphorus trifluoride studied by gas electron diffraction. Inorg. Chem. 1969, 8, 867–871.
70. Hartl, H.; Rama, M. Die Kristallstruktur von Phosphortrichlorid bei −110 °C/The Crystal Structure of Phosphorus Trichloride at −110 °C. Zeitschrift für Naturforschung B 1979, 34, 1035–1036.
71. Enjalbert, R.; Savariault, J.M.; Legros, J.P. Etude Structurale a 123 K du Trichlorure de Phosphore PCl3. Comptes Rendus de l'Académie des Sciences 1980, 290, 239–241.
72. Enjalbert, R.; Galy, J. Structure cristalline du tribromure de phosphore a 193 K. Acta Crystallogr. B 1979, 35, 546–550.
73. Lance, E.T.; Haschke, J.M.; Peacor, D.R. Crystal and molecular structure of phosphorus triiodide. Inorg. Chem. 1976, 15, 780–781.
74. Varadwaj, P.R.; Varadwaj, A.; Marques, H.M. Halogen Bonding: A Halogen-Centered Noncovalent Interaction Yet to Be Understood. Inorganics 2019, 7, 40.
